Particle Size Dependency of Ternary Diagrams at the Nanometer Scale: Evidence of TiO_2 Clusters in Fe-Based Spinels

N. Millot,[†] D. Aymes,[†] F. Bernard,[†] J. C. Niepce,[†] A. Traverse,[‡] F. Bourée,[§] B. L. Cheng,[||] and P. Perriat*,[⊥]

Laboratoire de Recherches sur la Réactivité des Solides, UMR 5613 CNRS/Université de Bourgogne, BP 47870, 21078 Dijon Cedex, France, Laboratoire pour l'Utilisation du Rayonnement Electromagnétique, UMR 130 CNRS, Bât. 209A, 91898 Orsay Cedex, France, Laboratoire Léon Brillouin, CEA-CNRS, CEA-Saclay, 91191 Gif-sur-Yvette Cedex, France, IRC in Materials Processing, The University of Birmingham, Edgbaston B15 2TT, United Kingdom, and Groupe d'Etudes de Métallurgie Physique et de Physique des Matériaux, UMR 5510 CNRS-INSA de Lyon, Bâtiment Blaise Pascal, 7 avenue Jean Capelle, 69 621 Villeurbanne Cedex

Received: October 25, 2002; In Final Form: February 5, 2003

The bulk (Fe,Ti,O) phase diagram is strongly modified at the nanometer scale: instead of the mixture of the rhombohedral and pseudo-brookite phases normally present in the micrometer range, a single fcc phase is stabilized for grain size lower than 25 nm. The existence of a single phase permits the formation of small TiO_2 clusters, which cannot happen in micrometer scaled compounds because of cluster growth until phase separation. Such clusters have been studied with techniques revealing order at different ranges. With diffraction experiments (revealing long range order), it has been shown that the crystallographic coherence between the fcc phase and the clusters is broken. With absorption spectroscopy experiments (revealing short range order), it was evidenced that the clusters consist of a compact stack of 4 TiO_2 entities. The presence of the fcc matrix around the clusters leads then to a new magic number of 4. This corresponds to a very stable configuration of clusters constrained to reside in an embedding fcc structure.

Introduction

The field of nanoparticles in materials research has sparked intense interest in expectation that this unexplored range of materials dimensions will yield drastic size-dependent properties.[1] One of the main surprising phenomena appearing in the nanometric range is the possibility of grain size driven phase transitions.[2] These transitions lead to very innovative materials since the materials resulting, stabilized by surface energies, paradoxically present both a high temperature structure and a very fine microstructure free from the defects generally induced by the predominant entropy term at high temperature. Examples are nanocrystalline cubic $BaTiO_3$ whereas the stable phase is tetragonal in monocrystals,[3] cubic Fe_2O_3 (instead of rhombohedral),[4] tetragonal ZrO_2 (instead of monoclinic),[5] and monoclinic Y_2O_3 (instead of cubic).[6] The more complete study of such transitions with complete experimental[7] and theoretical[8] determination of both surface and bulk energies concerns the corundum/spinel transition in Al_2O_3.[9] Some of the grain size driven transitions are even industrially exploited: it is the case for ZrO_2 which is largely used for mechanical reinforcement of ceramics or Fe_2O_3 for magnetic recording.

However, size driven phase transitions have been very rarely studied in ternary systems. Anyway, it can be expected that very spectacular modifications of the phase equilibrium diagram may be observed in compounds presenting some phase separation at a macroscopic scale. Indeed, since the contribution of the interface energy between the phases increases when the particle size decreases, the phase separation would cost more and more energy when reaching the nanometric range and a transition from a multiple- to a single-phase compound may occur. In this paper it is the nanoscale miscibility of a titanium ferrite presenting two phases at the macroscopic level which is studied. Apart from the paleomagnetic interest of titanomagnetites, which are found in the earth's crust as nanometer-scaled clusters,[10,11] and the recent evidence of a Verwey transition temperature shift in nanostructured Ti ferrites,[12] the choice of this material is motivated by several reasons. First, it is possible to determine unambiguously the exact influence of surface energies upon the structure since the ternary diagram (FeO, Fe_2O_3, TiO_2)[13] has been carefully determined in the case of monocrystals and some preliminary experiments have shown that the structure of titanomaghemite particles smaller than $\approx$ 20 nm effectively differs from that of monocrystals−it is a spinel (fcc) phase that is stabilized. Second, there is a good knowledge of the cation distribution in the spinel phase. Among the two types of sites occupied by the cations in the spinel,[14] tetrahedral (A), or octahedral (B), the Ti^{4+} cations reside only on octahedral sites whatever the scale, micrometer[15,16] or nanometer-sized.[17] Only when the Fe cations are not completely oxidized, the location of the Fe^{2+} cations is still subjected to controversial discussions.[18−20] Third, it is possible to study the size dependency of the phase diagram without any parasite variation of the oxygen composition. Indeed, in Fe-based spinels containing titanium (Ti/Fe = $x/3-x$), the equilibrium deviation from oxygen stoichiometry δ does not vary under air in a large temperature range (the oxido-reduction state of Ti is Ti^{4+} and that of Fe is Fe^{3+}). In the

* Corresponding author: e-mail: Pascal.Perriat@insa-lyon.fr.
[†] Université de Bourgogne.
[‡] Laboratoire pour l'Utilisation du Rayonnement Synchrotron.
[§] Laboratoire Léon Brillouin.
[||] The University of Birmingham.
[⊥] Groupe d'Etudes de Métallurgie Physique et de Physique des Matériaux.

10.1021/jp022312p CCC: $25.00
Published on Web 05/28/2003

TABLE 1: δ and Particle Size Inferred from X-ray Patterns Broadening in the Samples $(Fe_{3-x}Ti_x)_{1-\delta}O_4$ Annealed for a Long Time

	$(Fe_3)_{1-\delta}O_4$	$(Fe_{2.75}Ti_{0.25})_{1-\delta}O_4$	$(Fe_{2.50}Ti_{0.50})_{1-\delta}O_4$	$(Fe_{2.25}Ti_{0.75})_{1-\delta}O_4$	$(Fe_{2.00}Ti_{1.00})_{1-\delta}O_4$
δ	0.111	0.135	0.158	0.179	0.2
particle size (nm)	8 ± 1 nm	10 ± 2 nm	15 ± 2 nm	13 ± 2 nm	16 ± 2 nm

TABLE 2: Ti/Fe Ratio in the Samples $(Fe_{3-x}Ti_x)_{1-\delta}O_4$ Annealed for a Long Time[a]

	Ti/Fe				
$(Fe_{3-x}Ti_x)_{1-\delta}O_4$	theor.	EDS	ICP	EELS	XPS
0.25	0.091	0.08 ± 0.02	0.09 ± 0.01	0.09 ± 0.01	0.09 ± 0.02
0.50	0.2	0.18 ± 0.02	0.21 ± 0.01	0.21 ± 0.02	0.22 ± 0.02
0.75	0.33	0.33 ± 0.02	0.33 ± 0.01	0.32 ± 0.33	0.33 ± 0.03
1	0.5	0.49 ± 0.02	0.52 ± 0.01	0.48 ± 0.04	0.50 ± 0.04

[a] Analysis obtained from (i) energy dispersive spectrometry (EDS) in a JEOL JSM-6400F microscope, (ii) inductively coupled plasma (ICP) atomic emission spectrometry, (iii) electron energy losses spectroscopy (EELS) in a JEOL 4000 FX[51], and (iv) X-ray photoelectron spectroscopy (XPS) with a Riber Mac2 semi-imaging analyzer using 300 W Al Kα radiation.

chemical formula $(Fe_{3-x}Ti_x)_{1-\delta}O_4$, so written to express the fact that the main defects are cation vacancies, δ is equal to $(1 + x)/(9 + x)$. Obvious complications should have arisen with Mn−Zn ferrite[21] or Cu ferrite[22] samples, for which Mn^{2+}/Mn^{3+}, Mn^{3+}/Mn^{4+}, or Cu^{+}/Cu^{2+} ratios drastically vary with temperature under usual oxygen atmospheric conditions. Fourth, it is possible to study samples with unusually high contents of vacancies defects. In micrometer sized spinels indeed, only small deviations from oxygen stoichiometry can be achieved without phase transformation. In magnetite, for instance, the fcc phase undergoes a transformation to a rhombohedral one for $\delta > \delta_c = 0.0039$. In nanoscaled compounds on the contrary, the stability field of the fcc structure is strongly increased and very high defect contents in the fcc phase are expected, especially if the spinel contains cations with high valences. For example, the proportion of cation vacancies present in the structure increases from 11.1% for Fe_2O_3 ($\delta = 0.111$) up to 20% for $(Fe_2Ti)_{0.8}O_4$ ($\delta = 0.2$). Defect contents 50 times greater than for micrometer sized samples can then be obtained in nanoscaled Ti ferrites.

The expected change of the phase diagram at the nanometer scale immediately gives rise to another question, that of a possible modification of the arrangement of the atoms inside the newly obtained structure. The question is particularly open in the case of Ti ferrites: it may be expected that the interactions between the Ti and Fe cations, which leads to a phase separation at a macroscopic scale, modify the distribution of the cations inside the single phase obtained at the nanometer scale. One may then expect the existence of small clusters containing only TiO_2 groups. In the present case, these local Ti enrichments should lead to a local modification of the spinel structure. Indeed if small clusters rich in titanium were formed in $(Fe_{3-x}Ti_x)_{1-\delta}O_4$, which already contains a great amount of vacancies, a still larger number of vacancies should gather around the Ti^{4+} cations to preserve local electroneutrality and the spinel structure may locally collapse. Strictly speaking it is this local modification of the structure which would allow to describe the Ti assembly as a cluster. Such clusters may be then evidenced by appropriate diffraction techniques. Indeed, the diffraction patterns of the fcc phase should indicate a decrease of the Ti content when analyzed by the Rietveld method. For the determination of the Ti/Fe-ratio in the remaining spinel phase, neutron and anomalous X-ray diffraction have been carried out. Neutron diffraction allows efficient discrimination of the Fe and Ti cations since their nuclear scattering lengths strongly differ. The same discrimination can be achieved with anomalous X-ray diffraction when using different energies around the K edges of Ti and Fe.

The paper has then a double objective: first the study of the modification of a ternary diagram when the macroscopic scale is shifted to the nanometer range; second, that of the fluctuations in the local structure of the single phase stabilized by surface energies. It is then divided in two parts. The first one deals with the stabilization of new phases in a nanosized (Fe,Ti,O) system with evidence of the existence of a pure spinel phase below 25 nm. The second part concerns the study of the chemical fluctuations in the unique fcc phase obtained at the nanometer range: these fluctuations are inferred from diffraction techniques that investigate the long distance order and directly evidenced by absorption spectroscopy sensitive to the local environment of the atoms.

Investigated Materials

Preparation of Samples with and without Clusters Rich in Ti. Five compositions of titanium ferrites $(Fe_{3-x}Ti_x)_{1-\delta}O_4$ corresponding to $x = 0$, 0.25, 0.5, 0.75, and 1 have been synthesized according to a classical chemistry procedure. After dissolution of suitable amounts of ferrous, ferric, and titanium chloride (cations concentration $\approx$ 0.3 mol/l; pH $<$ 1), this mixture is added to an ammonia solution leading to instantaneous precipitation of titanium ferrites. During the reaction, the system is continuously stirred at 800 rpm. In accordance with the Ti and Fe solubility constants, the precipitate composition is the same as in the liquid phase. The particles are then separated by centrifugation at 3500 rpm for 5 min and washed with deionized water under ultrasonication for 5 min followed by a new centrifugation. After four successive washings, a sol is formed with neither surfactant nor dispersant addition. The sol is freeze-dried leading to a dry spinel precipitate as characterized by both X-ray diffraction experiments and IR spectroscopy measurements. Calcination in optimized conditions is carried out to eliminate remaining impurities and oxidize all the Fe cations while limiting crystalline growth: it consists of a thermal treatment for 10 h under air at 380 °C for $0.25 \leq x \leq 1$ and 330 °C for $x = 0$ after a ramp of 10 °C/h. All the obtained powders whose physical characteristics are detailed in Table 1 have a particle size around 10 nm. Their chemical composition has also been checked by a large variety of techniques: chemical analysis, electron dispersive spectroscopy, and electron energy losses spectroscopy (EELS). All these techniques (Table 2) have confirmed that the compositions obtained are in good agreement with those expected from the quantities of cations introduced during the process.

A temperature of 380 °C is just above the threshold of mobility of the Ti cations. It is only then when the temperature is maintained for a long time at 380 °C that some Ti clusters are expected to be formed. Other annealings with a duration

limited to 15 min have also been performed for $x = 0.25$, 0.5, 0.75 with the hope to obtain samples without clusters. We have then tried to prepare two series of samples with the same chemical formula, with the same degree of oxidation for the Fe cations, and with the same unique fcc phase, one containing and the other not containing clusters rich in titanium.

For comparison with titanium ferrites, an iron-chromite with the formula $(Fe^{3+})_A(5/3\ Cr^{3+}\ 1/3\ Vacancies)_B O_4^{2-}$ has also been prepared by the same soft chemistry route before annealing under air at 450 °C for 10 h. Similarly, a Zn−ferrite, $(Zn^{2+})_A(2Fe^{3+})_B O_4^{2-}$ has been prepared at high temperature (1200 °C) using the classical ceramics route. Finally, an annealing in reducing H_2/H_2O conditions at 400 °C has also been performed on a Ti−ferrite with $x = 0.5$: a powder with formula $(Fe_{2.50}Ti_{0.50})O_4$ and a grain size of 35 nm has then been obtained.

Control of the Deviation from Oxygen Stoichiometry: A Key Point for the Present Experiments. For all the samples prepared, obtaining well determined degrees of oxidation for the Fe cations present in the structure (i.e., well determined deviations from oxygen stoichiometry δ) is a key point for further interpretations. This has been achieved from the knowledge of the mechanisms responsible for cation oxidation in Fe-based spinels. It has been already shown indeed that the kinetics for oxidation involve two different processes.[23] First (i) there is some oxygen transfer at the gas/solid interface consisting of oxygen adsorption from the gas phase and incorporation into the lattice. During this step, new unit cells are formed on the surface with a change in the valence of the cations and creation of vacancies. Then (ii) there are diffusion processes of vacancies from the surface to the bulk counterbalanced by diffusion of cations toward the surface. Under usual temperature and oxygen partial pressure conditions, it is step (ii) which limits the whole process: the temperature for oxidation depends then on the mobility of the oxidizing cations within the spinel structure. In nanometer sized spinels, the mobility of the Fe cations becomes significant as early as 100 °C, and in Ti ferrites with a particle size less than 10 nm, it has been shown that the Fe oxidation took place entirely below 275 °C. Therefore, there is no doubt that whatever the duration of the above annealings, all the Fe cations are oxidized to Fe^{3+} after heating to 380 °C. In the present paper, the degree of oxidation of the Fe cations has been precisely verified using anomalous diffraction at the edges of the Fe^{2+} and Fe^{3+} cations.

Experimental Techniques

X-ray Absorption. X-ray absorption measurements were performed at the D42-XAS station of LURE-DCI. The signal was recorded at the Ti K (4965 eV) and the Fe K (7112 eV) edge using the total electron detection yield mode: it consists of the ratio of the current I generated by the electrons emitted from the samples during interaction with an incident photon beam current I_0 generated in an ionization chamber. To obtain the X-ray absorption near-edge structures (XANES), data were recorded at energy intervals of 0.5 eV in the range of 200 eV using a Si(331) two-crystal monochromator for Fe and a Si(311) one for Ti. Data were also recorded with a Si(111) two-crystal monochromator at intervals of 2 eV in the range of 1000 eV above the edge to obtain the absorption spectra from which the extended X-ray absorption fine structure (EXAFS) oscillations were extracted. XANES within 50−200 eV of threshold are known to be rich in chemical information. In the case of titanium, it even allows the Ti site symmetry to be deduced.[24] EXAFS was fitted to provide local crystallographic information (number and distance of the nearest neighbors) around the Ti and Fe cations using the code developed by Michalowicz.[25,26] The fitting procedure was here complicated by some remaining undetermination about the chemical nature (Ti or Fe) of the cationic neighbors residing on B sites. Indeed the oscillatory EXAFS function depends on the scattering phase shifts in the absorber and in the backscatterer and on a backscattering amplitude characteristic of the backscatterer.[27] However, both the backscattering amplitude for Fe and Ti cations and their respectively suffered phase shifts were very close when calculated according a McKale procedure:[28] simulations using Ti or Fe cations as backscatterer showed that they lead to less than 2% difference on the number of neighbors obtained. Since the majority of the cations are Fe ones in the spinel studied, the backscattering amplitude and phase were calculated assuming that the backscatterer is an Fe cation. Uncertainties upon the number of neighbors obtained by theoretical extraction from experimental data have been finally determined with calibrated samples: they are equal to ±3% for the third first shells and to ±10% for the fourth shell: they are less important than the ±10% generally admitted.

Neutron Diffraction. Neutron diffraction data were obtained at Laboratoire Léon Brillouin on the 3T2 2-axis spectrometer ($\lambda = 0.12253$ nm) or at Institut Laue Langevin on the D1B beam ($\lambda = 0.128$ nm).

X-ray Diffraction. X-ray diffraction (XRD) experiments were carried out using a D5000 diffractometer (Siemens) with a monochromatic Cu−Kβ wavelength ($\lambda = 0.13922$ nm).

Anomalous X-ray Diffraction. Anomalous X-ray diffraction has been performed on the D2AM-CRG beamline of ESRF using different energies around the K edges of Fe (7122, 7126, 7130, 7134 eV) and Ti (4981 eV). Around the edge of a cation present in the structure, the total structure factors strongly depend on the incident energy. Then the evolution of the diffraction patterns with energy provide quantitative information about the content of the considered cation on each site of the structure. Such a site-selective spectroscopy study has been already validated in the case of Ti ferrites by comparing the so-obtained cation distribution with that obtained by thermogravimetric analysis.[17] The anomalous dispersion contribution to the structure factor F, whose normal value is f_0, consists of additional real (f') and imaginary (f'') terms depending on the energy E according to the relation: $F = f_0 + f'(E) + if''(E)$. Using a sample with a well-characterized Fe/Ti-ratio, f'' can be directly calculated from X-ray absorption measurements:

$$f''(E) = \frac{mc}{2he^2N} E\mu(E)$$

The term $f'(E)$ can then be derived from $f''(E)$ by use of the Kramers−Kronig relation. In previous formulae, m is the electron mass, c the light velocity, h is Planck's constant, e the electron charge, and N the density number of atoms of the reference sample. The values of f' and f'' have been obtained by calibration with magnetite and different Ti ferrites.[29]

X-ray, anomalous X-ray, and neutron diffraction patterns have been analyzed by means of Rietveld refinements using the program FullProf.[30] Diffraction line profile analysis was also performed in order to determine the average crystallite size (size of a region over which the diffraction is coherent) and the crystallographic imperfections[31] (microdistortions, stacking faults, planar defects, etc.). The experimental profile for the peaks was Voigtian:[32] after instrumental corrections obtained from an annealed BaF_2 reference, the broadening was given by the formula $\beta^{*2} = (\beta^*/\epsilon) + \eta^2 d^{*2}$, where β is the integral width, ϵ the parameter linked to crystallite size and shape, η the

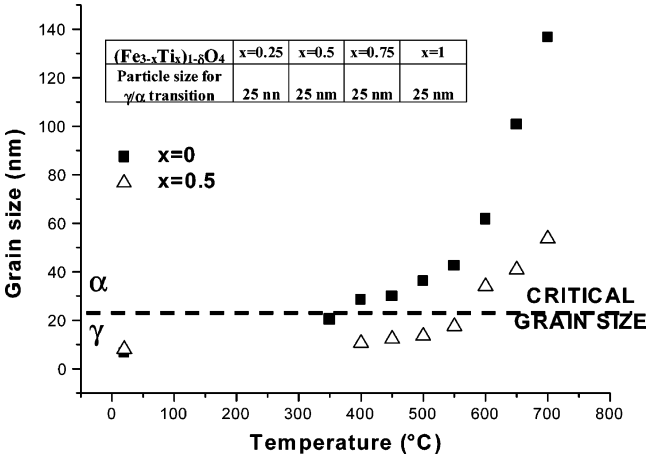

Figure 1. γ/α transition in $(Fe_{3-x}Ti_x)_{1-\delta}O_4$. In the samples with $x = 0$ and $x = 0.5$, the grain size has been increased by annealing at a heating rate of 2 °C/min up to different temperatures. The nature of the phase, γ or α, has been determined by X-ray diffraction and the grain size calculated from the patterns broadening. (inset) Determination of the critical grain size by dilatometric experiments (the temperature for transition is given by a breakdown in the densification curves; the critical grain size is then determined by examination of samples quenched just below and above the transition). Uncertainties upon the grain size is ±10%.

parameter linked to strain. $\beta^* = \beta\cos\theta/\lambda$ and $d^* = 2\sin\theta/\lambda$ are the reduced coordinates depending on the diffraction angle θ and on the wavelength λ.

Evidence for Size-Driven Transitions in the (Fe,Ti,O) System: Stabilization of a Pure Spinel Phase

The first objectives of the paper are to provide evidence that in the nanometer range a pure spinel phase is effectively stabilized by surface energies and to characterize the domain of stability of this new phase. First experiments were then carrying out for determining the evolution with particle size of the crystalline structure of powders of maghemite and of titanium ferrites. This has been made by studying the X-ray diffraction and IR spectroscopy[33−35] fingerprints of samples heated under air at a linear rate of 2 °C/min and quenched. The starting powders had the spinel structure and were characterized by a particle size of around 10 nm. From Figure 1 it appears that, whatever in the case of $(Fe_3)_{0.889}O_4$ (Fe_2O_3-maghemite) or $(Fe_{2.50}Ti_{0.50})_{0.842}O_4$, a transition from the spinel to the rhombohedral phase is observed. In the case of the ferrite containing Ti, it is quite surprising since the state which is stable at the macroscopic scale is not a pure rhombohedral phase but a mixture of pseudobrookite and rhombohedral phases. The fact that a single phase is obtained is explained by the argument that, at the nanometer scale, interfaces energy becomes prohibitive in multiple phases mixtures. Transformation to a rhombohedral/pseudobrookite mixture will be achieved only for largely higher temperatures (above 750 °C) after significant increase of the grain size (> 150 nm).

From Figure 1, it appears that the critical grain size for which the fcc (γ)/rhombohedral (α) transition is observed is, in both cases, equal to 25 ± 2 nm. It is still the same regardless of the Ti content, 0.25, 0.5, 0.75, or 1, as shown in the inset of Figure 1, which relates some additional determination of the critical grain size by dilatometric experiments. The value of 25 nm is consistent with that obtained previously in the case of Fe_2O_3.[4] In contrast, the temperature, $T_{\gamma/\alpha}$, at which the γ/α transition occurs is about 200 °C higher for the titanium ferrite $(Fe_{2.50}Ti_{0.50})_{0.842}O_4$ ($T_{\gamma/\alpha} \approx 590$ °C) than for maghemite ($T_{\gamma/\alpha} \approx 410$ °C). These two results can be explained by a combination of thermodynamics and kinetics considerations. Indeed, the transition parameters (temperature, grain size) are given by the equality of the Gibbs potential (which contains surface and volume terms) between the two phases. This equality consists of the following implicit relation between the critical grain size, D_{critical}, and the critical temperature, $T_{\gamma/\alpha}$:[36,37]

$$D_{\text{critical}} = -6\bar{V}(\gamma_\gamma - \gamma_\alpha)/(\mu^0_\gamma(T_{\gamma/\alpha}) - \mu^0_\alpha(T_{\gamma/\alpha}))$$

In this relation, $\bar{V}$ is the molar volume, γ the surface energy and $\mu^0_\alpha = -196.5 - 21.5\ T$ kJ/mol and $\mu^0_\gamma = -267.0 - 35\ T$ kJ/mol the chemical potentials[38] of the two phases. Between 410 and 590 °C, the $\mu^0_\gamma - \mu^0_\alpha$ decrease is of 26% whereas that of $\gamma_\gamma - \gamma_\alpha$ is around 20% (the temperature dependence of the surface energies is around 10^{-3}/K). If one assumes that the thermodynamic quantities μ^0 and γ are not strongly dependent on the Ti composition, that implies that the grain size at transition does not vary significantly with the temperature at which the transition occurs. It is exactly what is observed. Therefore, the temperature for transition is only determined by the particle growth during heating to the size of $D_{\text{critical}} \approx 25$ nm. This activation temperature depends on the kinetics of the particle growth and is now dependent on the Ti content of the spinel. Indeed, the Ti cations have a lower mobility than the Fe ones in the spinel structure. The difference in the diffusion rate of these cations can be explained by the difference in their distance to the nearest oxygen, $d_{\text{cation}-O}$ in the fcc structure ($d_{Ti_B^{4+}-O} = 1.944$ Å; $d_{Fe_B^{3+}-O} = 2.020$ Å[39,40]). Indeed the mobility of a cation is related to the electrostatic interactions with its oxygen neighbors: then the smaller the distance $d_{\text{cation}-O}$, the higher the interactions with the anions and the higher the energy barrier to be crossed over in a diffusion jump.

Evidence of TiO_2 Clusters Without Crystallographic Coherence with the Surrounding fcc Phase

Evidence by Diffraction that All the Ti Cations Are Not in the Unique fcc Phase Observed: Existence Of A Non-diffracting Phase Containing these Extra Ti Cations. The unique spinel phase stabilized by surface energy is now studied in detail by diffraction techniques, with the objective to evidence the presence of clusters in the samples investigated. As explained previously, the formation of clusters rich in Ti should be accompanied by some collapse of the fcc phase due to an excessive aggregation of vacancies around the gathered Ti^{4+}. Then the so-formed clusters should not contribute to the patterns of the fcc phase, and the Ti/Fe ratio in the remaining fcc phase should significantly decrease. Diffraction has then been carried out on samples submitted to different annealing durations. Only for the prolonged annealing of 10 h are some clusters expected to be formed.

It is from simultaneous Rietvelt refinements[41] of neutron and X-ray diffraction patterns that the Fe and Ti distribution in the fcc phase has been determined. The refined structure corresponds to that of the $Fd\bar{3}m$ space group (no. 227 in ITC numeration[42]) with a cubic cell containing 192 atoms. The X-ray atomic Thomson (elastic) scattering factor is proportional to the number, Z, of electrons of the atom considered, which is approximately the same for Fe ($Z = 22$) and Ti ($Z = 26$);[43] then the X-ray diffraction pattern analysis mainly allows the quantification of the vacancies contents. On the contrary, the nuclear neutron scattering lengths, b, of Ti ($b_{Ti} = -0.3438 \times 10^{-12}$ cm) and Fe ($b_{Fe} = 0.9450 \times 10^{-12}$ cm)[44] differ very strongly. Neutron diffraction is then appropriate for the determination of the Fe/

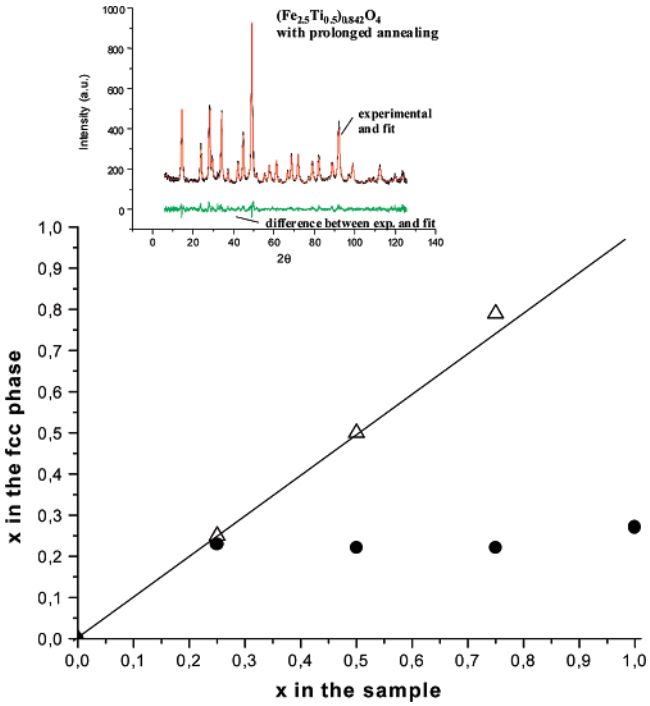

Figure 2. Determination of the Ti content x in the fcc phase as a function of that in the samples $(Fe_{3-x}Ti_x)_{1-\delta}O_4$ for limited (△) or prolonged (●) annealings. When the samples are shortly annealed, all the Ti cations are in the fcc phase. When the samples are annealed for a long time, there is formation of a nondiffracting phase rich in Ti. (inset) Example of Rietveld refinements of neutron diffraction patterns showing the experimental data, their fit, and the difference between the experiments and the fit.

Ti ratio. Additional constraints in the structural refinement such as electroneutrality or the fact that the Ti^{4+} cations reside only on the B sites have been taken into account. Finally, for fitting the neutron diffraction patterns, the magnetic structure had also be considered: the cubic magnetic cell was found in coincidence with that of the $Fd\bar{3}m$ space group and, inferred from the absence in the neutron diffraction patterns of the 200 and 644 Bragg peaks,[45] the magnetic structure was ferrimagnetic. An example of refinements of neutron diffraction patterns is given in the inset of Figure 2, and the structural information relative to the cationic distribution is given in Table 3.

Unsurprisingly, the cation distribution determined in the samples submitted to a short annealing at 380 °C coincides with that expected when all the Fe and Ti cations present in the sample are distributed on the sites of the fcc phase. This confirms that, at the nanometer range, it is possible to obtain spinel phases having very high vacancy contents. However, the main result concerns the samples submitted to a prolonged annealing for which there is a strong discrepancy between the titanium content in the sample and that found in the single fcc phase. Whereas the agreement between the two titanium contents is pretty good for $x = 0.25$, the difference between them significantly increases with x. In all the samples annealed, the composition in the spinel phase is approximately the same as it would exist with a titanium solubility limit around the composition $x = 0.25$. This result then clearly shows that part of the Ti cations are out of the coherent spinel lattice within a second phase which does not provide any contribution to diffraction. It is this second phase resulting from the collapse of a part of the fcc phase rich in Ti that will be claimed further to consist of small clusters containing Ti.

To confirm the collapse of a part of the fcc lattice, the cation distribution of the sample submitted to a prolonged anealing

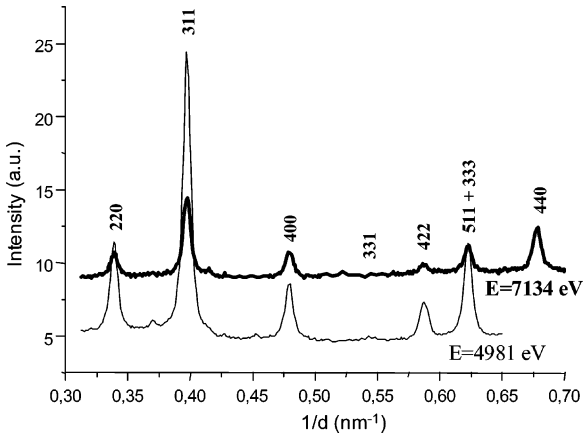

Figure 3. Anomalous X-ray diffraction patterns at energies around the FeK (7134 eV) and TiK (4981 eV) edges in the case of the powder $(Fe_{2.5}Ti_{0.5})_{0.842}O_4$ annealed for a long time. Note that the background and the relative intensities of the peaks are modified when changing the energy.

has been verified, for the compositions $x = 0.5$ and $x = 0.75$, by a series of anomalous diffraction recordings at different energies around the FeK edge and just after the TiK edge. To interpret such results, it must be considered that the diffraction pattern intensities depend on the location of the cations in the spinel structure: for instance the 220 and 422 peaks depend mainly on the cations on the A sites, whereas the 311, 400, 511, 333, 440, 620, and 533 peaks depend on the cations located on both types of sites. Moreover, at different wavelengths the diffraction patterns depend also on the nature of the cations: just a few eV above the TiK edge ($E_{X-rays} = 4981$ eV $> E_{TiK} = 4965$ eV) the Ti cations have a very weak contribution to the elastic scattering (compared with the Fe ones), whereas it is the contrary above the FeK edge ($E_{X-rays} = 7122$, 7126, 7130, and 7134 eV). This explains why, as seen in Figure 3, the 220 and 422 peaks have, compared with the 400 one, relatively higher amplitudes with $E_{X-rays} = 4981$ eV than with energies around the FeK edge. Indeed, the Ti cations only residing on B sites do not provide any contribution to the 220 and 422 peaks, and then do not contribute to their attenuation at the TiK edge. Note also that, consistent with the increased inelastic diffusion, the elastic scattering/background ratio significantly decreases around the FeK edge. From simultaneous Rietveld refinements at all the analysis energies, the cation distribution has been determined (Table 3); it confirms distribution previously determined from X-ray (at CuKβ radiation) and neutron diffraction.

Finally, since anomalous diffraction at the edges of the Fe cations are sensitive to the Fe valence, it has been used in the case of $x = 0.25$ to verify that all the Fe cations were oxidized to Fe^{3+}, even for the shorter annealings. This appears clearly in Table 3, showing that the presence of Fe^{2+} has to be definitely left out in all the investigated samples.

Evidence that the Nondiffracting Phase Is Finely Dispersed Within the Particles. After having proved that all the Ti cations do not reside on the fcc lattice, it is necessary to determine the location of the nondiffracting phase containing the extra Ti cations. Since X-ray photoelectron spectroscopy (XPS) is a technique sensitive to the surface, it may provide some information about the possible expulsion of some Ti cations from the bulk. In this case indeed, XPS should reveal an increase in the Ti/Fe ratio compared with stoichiometry. According to Table 2, absolutely no increase of the surface Ti content is detected in the samples annealed for a long time,

TABLE 3: Cation Distribution in the fcc Phase of the Powders Submitted to a Limited or a Prolonged Annealing[a]

		technique	x ±0.02	Fe_A ±0.03	$\square_A$ ±0.03	Fe_B ±0.03	Ti_B ±0.03	$\square_B$ ±0.03
$(Fe_3)_{0.889}O_4$	expected		0	1	0	1.667	0	0.333
	prolonged annealing	ND-LLB	0	0.98	0.02	1.68	0	0.32
$(Fe_{2.75}Ti_{0.25})_{0.865}O_4$	expected		0.25	1	0	1.375	0.22	0.405
	limited annealing	ND-ILL	0.25	0.94	0.06	1.43	0.22	0.35
		AD	0.25	0.95	0.05	1.43	0.22	0.35
	prolonged annealing	ND-LLB	0.23	0.96	0.04	1.48	0.20	0.32
		ND-ILL	0.23	0.96	0.04	1.48	0.20	0.32
$(Fe_{2.50}Ti_{0.50})_{0.842}O_4$	expected		0.5	1	0	1.104	0.421	0.475
	limited annealing	ND-ILL	0.5	0.92	0.08	1.18	0.42	0.40
	prolonged annealing	ND-LLB	0.22	0.93	0.07	1.48	0.19	0.33
		ND-ILL	0.20	0.96	0.04	1.47	0.17	0.36
		AD	0.20	0.97	0.03	1.47	0.17	0.36
$(Fe_{2.25}Ti_{0.75})_{0.821}O_4$	expected		0.75	1	0	0.84	0.62	0.54
	limited annealing	ND-ILL	0.79	0.70	0.30	1.10	0.65	0.25
	prolonged annealing	ND-LLB	0.22	0.88	0.12	1.53	0.19	0.28
		AD	0.22	0.91	0.09	1.49	0.19	0.32
$(Fe_{2.00}Ti_{1.00})_{0.8}O_4$	expected		1	1	0	0.6	0.8	0.6
	prolonged annealing	ND-LLB	0.27	0.85	0.15	1.51	0.23	0.26

[a] The distribution has been determined from anomalous X-ray diffraction (AD) or neutron diffraction performed at Institut Laue Langevin (ND-ILL) or Laboratoire Léon Brillouin (ND-LLB). The expected compositions are given in the case where the vacancies reside on the B sites only.

which permits to eliminate any interpretation involving some precipitation of a titanium-rich phase outside or at the surface of particles. This point had been confirmed by high resolution (0.17 nm) transmission electronic microscopy (TEM), which revealed the absence of fine particles in the powders observed. The nondiffracting titanium-rich phase is then homogeneously dispersed within the particle.

The question concerns now the spatial extension of this second phase containing the extra Ti cations. It is very unprobable that this phase can significantly extend in particles of 10 nm. Except for the fact that such an extension would lead to heterogeneities visible with XPS or TEM techniques, it would lead to net interfaces between the two phases, which is very unlikely in the nanometer range because of prohibitive energy. In the first part of the paper we have demonstrated that, up to 150 nm, the rhombohedral/pseudobrookite mixture normally existing at the macroscopic scale was replaced by unique phases: an fcc phase below 25 nm, a rhombohedral phase above. Admitting now the coexistence of two phases with similar extension within nanoparticles would be in contradiction with these considerations.

On the contrary, when considering that the spinel structure contains two types of cation sites, A and B, and that the Ti cations reside only in octahedral coordination, it is clear that clusters formed by some Ti aggregation should have a limited spatial extension. Since, moreover, a great amount of vacancies should gather around these Ti aggregates, it is more likely that the spinel structure will collapse at the place of these aggregates. In agreement with all previous observations, the Ti clusters may then be considered as blocks of a few atoms embedded in the fcc structure, albeit without crystallographic coherence with the fcc lattice. Such a situation, if verified, would be quite specific to the nanometer range.

Characterization of the Short Range Order in the Nondiffracting Phase: Evidence that the Nondiffracting Phase Consists of Small Clusters Containing Ti. To better examine the relevance of this proposition, experiments investigating the short-range order around the Ti cations have been carried out. Indeed, even if the nondiffracting phase appears amorphous with diffraction techniques, it must present some order at short distances. Then if the spatial extension of the short range order around the extra Ti cations was extremely limited, this should be assigned to a very small size of the nondiffracting phase with an additional indication of a broken coherence between the fcc and the second phases.

XANES and EXAFS have then been performed at the edges of Fe and Ti with the attempt to show successively that (i) there are no Fe cations in the nondiffracting phase, (ii) all the Ti cations in the non diffracting phase are in octahedral coordination, and (iii) the nondiffracting phase consists of small clusters.

(i) Proof by FeK−XANES and FeK−EXAFS that there Are No Fe Cations in the Nondiffracting Phase. It is from an eventual difference with the FeK−XANES characteristic of the spinel that the presence of some Fe^{3+} cations in the nondiffracting phase should be appreciated. Since the Fe^{3+} cations reside on the two types of sites of the fcc structure, the Fe^{3+}K−XANES of the samples annealed for a long time have been compared with those of a Zn ferrite, $(Zn^{2+})_A(2Fe^{3+})_BO_4^{2-}$ and of an iron chromite $(Fe^{3+})_A(5/3\ Cr^{3+}\ 1/3\ \text{Vacancies})_BO_4^{2-}$. With these two especially prepared samples indeed, one has standards in which the Fe^{3+} cations are entirely located on B sites (with Zn ferrite) or on A sites (with Fe chromite). The result of such comparison, Figure 4a, is that the overall shape and details of the FeK absorption spectra of the Ti ferrites investigated are perfectly intermediate between those of the Zn ferrite and of the Fe chromite. Such observations constitute strong arguments to prove that all the Fe cations present in the samples reside only on the A and B sites of the spinel structure. This conclusion is reinforced when one remarks that the Fe_B/Fe_A ratio in Table 3 is the same (≈ 1.5) within the fcc phase, regardless of the composition of the sample. Then only the presence of some Fe cations in the nondiffracting phase should induce a change in the Fe^{3+}K−XANES spectra when the proportion of the nondiffracting phase increases. Since all the spectra exactly coincide even for the higher Ti contents, the amorphous phase must contain only titanium cations.

An additional proof that the Fe cations are all in the spinel phase can be derived from the study of the FeK−EXAFS oscillations. Indeed, the pseudoradial functions (PRF) relative to the Fe cations show that, regardless of the composition of the ferrites annealed for a long time, the environment of the Fe cations is almost exactly the same (Figure 5) and is again

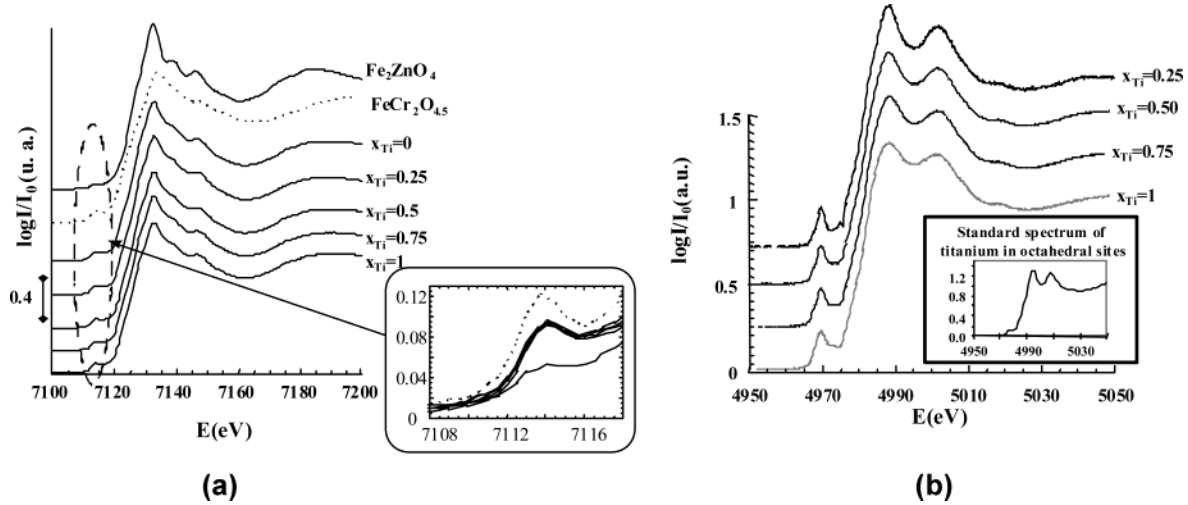

Figure 4. XANES in different titanium ferrites $(Fe_{3-x}Ti_x)_{1-\delta}O_4$ annealed for a long time. (a) XANES at the FeK edge with comparison of XANES of Fe_2ZnO_4 and $FeCr_2O_{4.5}$. (b) XANES at the TiK edge with in inset XANES of a standard Fe_2TiO_4.

TABLE 4: Numbers and Distances of the First Neighbors of the Fe Cations in Samples Annealed for a Long Time as Obtained by FeK−EXAFS and by Diffraction[a]

$(Fe_{3-x}Ti_x)_{1-\delta}O_4$		$x = 0$	$x = 0.25$	$x = 0.5$	$x = 0.75$	$x = 1$
first O neighbors	distance Å	1.96 ± 0.02	1.96 ± 0.02	1.96 ± 0.02	1.96 ± 0.02	1.96 ± 0.02
(EXAFS)	number	5.1 ± 0.1	5.1 ± 0.1	5.3 ± 0.1	5.1 ± 0.1	5.3 ± 0.1
first O neighbors	distance Å	1.96 ± 0.02	1.96 ± 0.02	1.96 ± 0.02	1.96 ± 0.02	1.96 ± 0.02
(diffraction)	number	5.3 ± 0.1	5.3 ± 0.1	5.3 ± 0.1	5.3 ± 0.1	5.3 ± 0.1

[a] In the case of diffraction, the quantities have been determined from the cation distribution given Table 3 by average on the A and B sites (the $Fe_A^{3+}-O$ and $Fe_B^{3+}-O$ distances are respectively 1.858 and 2.020 Å.[51]

TABLE 5: Bond Distances, Debye−Waller Factors and Coordination Numbers of the Successive Shells of the Ti Cations in (a) $(Fe_{2.50}Ti_{0.50})$ O_4, (b) $(Fe_{2.50}Ti_{0.50})_{0.842}O_4$ Submitted to a Limited Annealing, and (c) $(Fe_{2.50}Ti_{0.50})_{0.842}O_4$ Submitted to a Prolonged Annealing

		first neighbors O	second neighbors Fe or Ti on B sites	third neighbors Fe on A sites	fourth neighbors O
$(Fe_{2.50}Ti_{0.50})$ O_4	distance Å	1.98	3.07	3.59	3.80
	σ Å	0.10	0.11	0.13	0.19
	number	6.1 ± 0.2 (exp.)	6.05 ± 0.2 (exp.)	5.8 ± 0.2 (exp.)	7.3 ± 0.5 (exp.)
		6 (theo.)	6 (theo.)	6 (theo.)	8 (theo.)
$(Fe_{2.50}Ti_{0.50})_{0.842}O_4$	distance Å	1.98	3.09	3.43	3.58
after limited annealing	σ Å	0.11	0.11	0.13	0.21
	number	6.0 ± 0.2 (exp.)	4.6 ± 0.2 (exp.)	5.8 ± 0.2 (exp.)	8 ± 0.5 (exp.)
		6 (theo.)	4.8 (theo.)	5.6 (theo.)	8 (theo.)
$(Fe_{2.50}Ti_{0.50})_{0.842}O_4$	distance Å	1.98	3.07	3.43	3.60
after prolonged annealing	σ Å	0.12	0.13	0.17	0.40
	number	6.2 ± 0.2	2.45 ± 0.1	3.3 ± 0.1	4.2 ± 0.2
	number in fcc phase	2.4 ± 0.5	1.9 ± 0.3	2.3 ± 0.3	3.2 ± 0.5
	number in cluster	3.8 ± 0.6	0.55 ± 0.4	1.0 ± 0.4	1.1 ± 0.7

characteristic of the spinel phase. Again also, the PRF are intermediate between those obtained in the case of a Zn ferrite and that of an Fe chromite. In Zn ferrite, the Fe cations are surrounded by six anions, six cations on B sites at ≈ 3 Å, and six cations on A sites at ≈ 3.5 Å. In the case of the Fe chromite, they are surrounded by four anions and twelve cations residing on B sites at ≈ 3.5 Å. These differences in the coordination spheres explain the presence of fine double peaks in the PRF of the Zn ferrites and the presence of a slightly larger single peak in that of Fe chromite. They also explain why in the case of the titanium ferrites, only one peak characterized by a comparatively large half-width is observed. From the fit of the filtered contribution of the first shell extracted from the PRF, the characteristics of the first oxygen neighborhood of the Fe cations present in the samples have been determined. This information allows a confirmation that all the Fe cations are effectively in the fcc phase. Indeed, if there were some in the second phase, there would be a difference between the environment of the Fe cations determined by diffraction and that obtained by EXAFS (EXAFS is sensitive to all the Fe cations present in the sample, whereas diffraction takes into account those within the fcc phase). Table 4 displays the coordination number and the distance for the first oxygen shell found according to these two techniques. The excellent agreement between them confirms that the Fe cations are entirely on the sites of the fcc phase. This point is crucial since it eliminates the possibility of an Fe_2TiO_5-type phase, as in the macroscopic equilibrium phase diagram, and proves the absence of Fe cations in the nondiffracting phase.

(ii) Proof by TiK−XANES that Ti Is in Octahedral Coordination. After having demonstrated that the nondiffracting phase contains only Ti cations, more information about the environment of the Ti cations within this second phase can be obtained from TiK−XANES. The TiK−XANES are shown in Figure

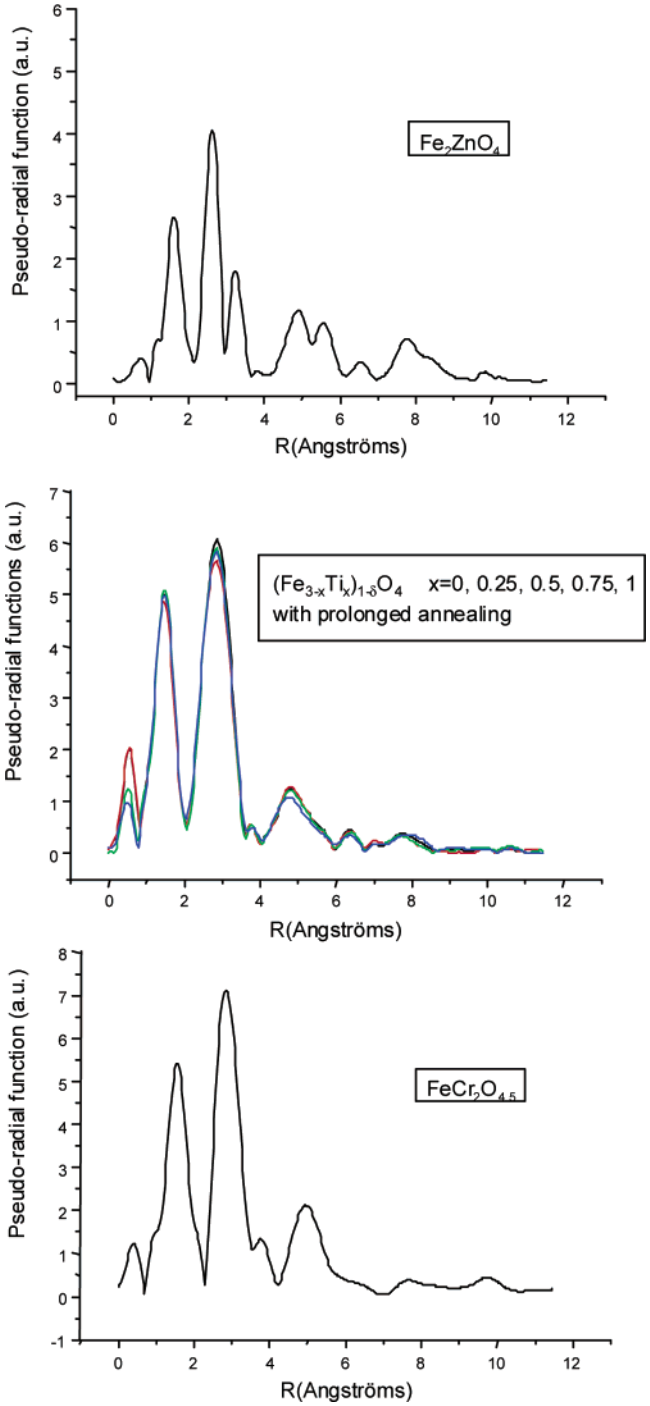

Figure 5. PRF around the Fe cations in the case of (top) Zn_2FeO_4, (middle) $(Fe_{3-x}Ti_x)_{1-\delta}O_4$ annealed for a long time, and (bottom) $FeCr_2O_{4.5}$.

4b for the samples annealed for a long time. For all these samples, the XANES are quite similar to that of titanium located on the B sites in the spinel structure, as one can see in the inset of Figure 4b. It is true regardless of the preedge assigned to the transition from the 1s to the 3d state[46] or the shape and the position of the double-peak between 4985 and 5005 eV related to the transition from the 1s to the np state.[47] Such a result may be easily understood in the case of the sample with the composition $x = 0.25$ since almost all the titanium cations belong to the spinel phase. However for $x > 0.5$, such a result is somewhat surprising since the majority of the titanium cations belongs to the nondiffracting phase. It implies that even if the nondiffracting phase has no crystallographic coherence with the

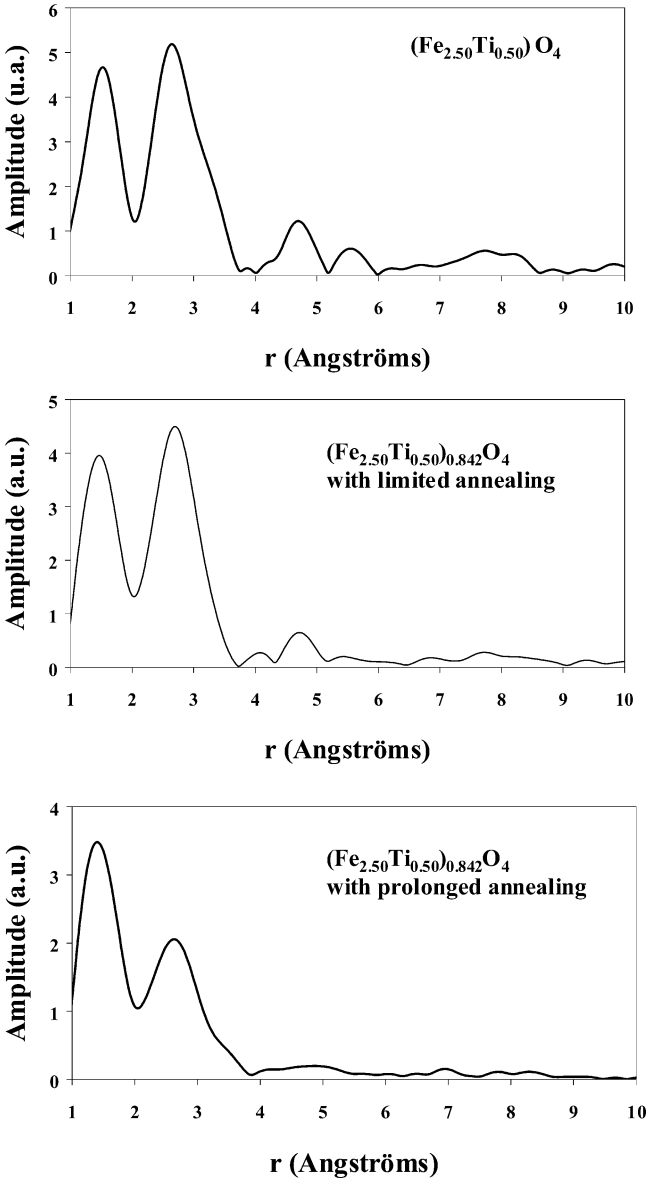

Figure 6. PRF around the Ti cations in (a) $Fe_{2.5}Ti_{0.5}O_4$, (b) $(Fe_{2.5}Ti_{0.5})_{0.842}O_4$ submitted to a limited annealing, and (c) $(Fe_{2.5}Ti_{0.5})_{0.842}O_4$ submitted to a prolonged annealing.

surrounding spinel phase, the chemical environment of titanium inside this second phase is quite similar to that existing in the B site of the spinel structure. This point reinforces the possibility of a process already evoked for the formation of a second phase within the particle. As schematically illustrated in Figure 8, it consists of aggregation of some Ti cations until a critical size for which the correlative accumulation of surrounding vacancies leads to a decoherency with the fcc phase. In such a mechanism, the relative arrangements of the atoms should not be modified compared to those in the fcc phase; however, the reduced number of bonds between the clustered Ti cations and the atoms of the fcc phase should become insufficient to a full determination of the position of the clustered atoms relative to those in the spinel lattice. This would explain why the environment of the clustered Ti cations remains the same as in the spinel, whereas the coherence between the phases would be lost.

(iii) Proof by TiK−EXAFS that the Nondiffracting Phase Consists of Small Clusters. For confirmation of such hypotheses and better characterization of the spatial extension of the clusters, the successive coordination shells of the Ti cations contained in the second phase have been extracted from the TiK−EXAFS

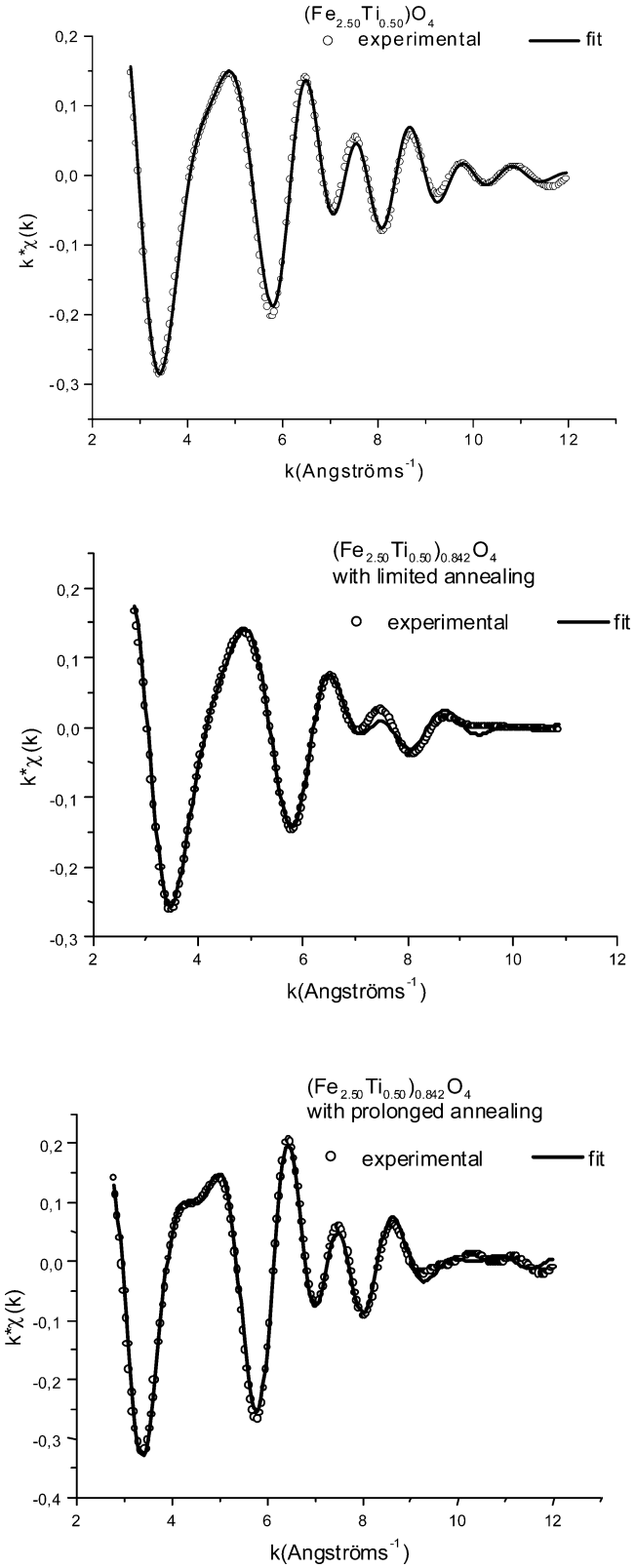

Figure 7. Comparison of experimental filtered Ti−PRF and their fits in (top) $Fe_{2.5}Ti_{0.5}O_4$, (middle) $(Fe_{2.5}Ti_{0.5})_{0.842}O_4$ submitted to a limited annealing, and (bottom) $(Fe_{2.5}Ti_{0.5})_{0.842}O_4$ submitted to a prolonged annealing.

oscillations. In the case of the investigated powder, $(Fe_{2.5}Ti_{0.5})_{0.842}O_4$, subjected to a prolonged annealing, the PRF relative to the Ti cations (Figure 6) exhibits strong differences with that relative to the Fe cations (Figure 5). Indeed, just after the first shell of oxygen neighbors around 2 Å, the pseudoradial function

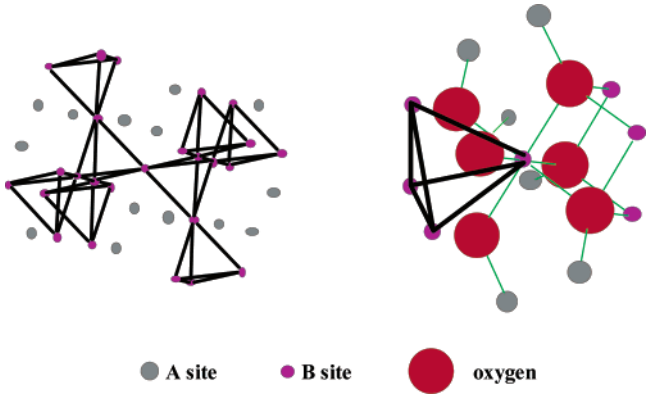

Figure 8. (left) Possible location of clusters containing four adjacent B sites in the spinel structure. (right) Bonds of a clustered cation with the fcc phase. For a clustered Ti cation in a four-membered cluster, there are 12 bonds between its surrounding oxygen and the cations in the fcc phase. If these cations are replaced by vacancies, the coherence with the spinel phase can be broken.

shows a large significant decrease. Even for amorphous phases, this decrease is unusually pronounced since in extended materials some short-range order may always be found. For instance, amorphous TiO_2 obtained by anodization locally presents the same structure as anatase, even with a complete Ti second neighborhood.[24] The drastic decrease of the PRF has then to be assigned to a very small extension of the phase containing the extra Ti cations. If there were no coherence between the phases indeed, this small size would perfectly explain the small number of second Ti neighbors. The decrease in the PRF should indicate then that (i) the coherence between the fcc and the second phase is broken, and (ii) the spatial extension of the second phase is strongly limited. If it were, this would also be consistent with the diffraction results.

To reinforce this interpretation, the PRF of the Ti cations has been compared to that relative to the same powder $(Fe_{2.5}Ti_{0.5})_{0.842}O_4$ with the same composition, and with the same deviation from oxygen stoichiometry but which has been subjected to only a short annealing. Strong differences immediately appear between the PRFs since the PRF relative to the shortly annealed ferrite presents the same characteristics as those of a stoichiometric spinel $(Fe_{2.5}Ti_{0.5})O_4$. This confirms first that the samples subjected to short annealings consist of a pure fcc phase. After a fit of the first four shells of the Ti cations (Figure 7 for the fit, Table 5 for the results), this confirms also that in samples shortly annealed the vacancies are homogeneously distributed on their respective sites of the fcc lattice. It is then only during further annealing at 380 °C that the clusters are formed. The nature of the order within the clusters can be specified from the Debye−Waller factors (Table 5). Between the Debye−Waller factors of the Ti cations within the pure spinel phase of the sample shortly annealed (0.11−0.13 Å for the first three shells) and those in the sample presenting clusters (0.12−0.17 Å), only a small increase is observed. That indicates a well-defined short-range order within the clusters and confirms that the decrease of the Ti PRF in the sample annealed for a long time mainly arises from a small number of atoms in the clusters. Then either the neighbors of the clustered Ti cations are in the fcc phase and they do not give any contribution to the PRF, or the neighbors are in the clusters and they participate in the PRF with an only slightly increased Debye−Waller factor. Definitive conclusions can then be drawn about the processes involved during annealing: as inferred from diffraction, a part of the Ti cations are losing coherence with the spinel structure

and, as proved by absorption, gather in clusters with a size smaller than 4 Å.

Determination of the Size of the Clusters. An accurate estimate of the size of the clusters can be obtained from the fit of the PRF involving different shells around the Ti cations. For such a fit, it was taken into account that the Ti cations reside either in the fcc phase (40 ± 4% according to the diffraction analysis) or in the clusters (60 ± 6%). For the 40% of the Ti cations in the fcc phase (with composition $(Fe_{2.79}Ti_{0.21})_{0.869}O_4$ see Table 3), the number of their first neighbors has been calculated from the theoretical structure of the bcc phase (no. 227 in ITC numeration) and the distances of the surrounding atoms have been identified to those experimentally found in the nonannealed sample $(Fe_{2.75}Ti_{0.25})_{0.865}O_4$. It is justified because this sample has a composition very close of $(Fe_{2.79}Ti_{0.21})_{0.869}O_4$ and consists of a pure fcc phase. It was then found that the 40% of the Ti cations residing in the spinel phase are surrounded by a first shell of 6 O at 1.98 Å, a second shell of 4.9 cations, Fe or Ti, on B sites at 3.10 Å, a third shell of 5.7 cations, Fe or Ti, on A sites at 3.45 Å, and a fourth shell of 8 O at 3.60 Å (Table 5). In such a result, no difference between the cation nature of the metallic neighbors, Fe or Ti, has been made, which is well-founded because of their very close backscattering amplitude and phase shifts.[28] For the 60% of the Ti cations contained in the clusters, the fit has then been made assuming that the distances of the different shells around the clustered Ti cations are the same as those in the spinel phase. This hypothesis is justified subsequently by the good fit of the experimental data. The distances and the numbers of the successive neighbors of the titanium cations in the clusters are given in Table 5. Despite relatively large uncertainties characteristic of EXAFS results, it appears that each cation in the clusters has around three neighbors at less than 3.5 Å. Such a value is very low compared with that of 10.6, which would have been obtained in the case of no cluster formation (10.6 takes into account the presence of vacancies on the two sites of the spinel structure). It indicates that each cluster should contain ≈ four cations.

Why Each Cluster Contains Four TiO_2 Groups. Such a value of four is in remarkable agreement with the possibility offered by the spinel structure for the formation of clusters constituted of cations forced to reside on the B sites only. As indicated in Figure 8 indeed, compact arrangements of four adjacent B sites separated by A sites can be easily found in the spinel structure. Since 60% of the Ti cations of the sample annealed for a long time are gathered in clusters, only eight of the so-described tetrahedral arrangements correspond to effective clusters, the others being normally occupied by the Fe and the remaining Ti cations.

Finally, the consistency of the so-given description is reinforced by the fact that, due to the large amount of vacancies aggregating around the clustered Ti cations, the crystallographic coherence between the cluster and the fcc phase is likely to be broken. As already mentioned the number of vacancies aggregating around the clustered Ti cations increases with the size of the cluster in order to counterbalance the high charge of the Ti cations. A critical size for which the spinel structure collapses may then be expected, and one may wonder if this critical size could correspond to a four-membered cluster. The Ti cations are related to the fcc phase via oxygen anions. A condition for coherence of a clustered Ti cation with the surrounding bcc phase is then that it is bounded to at least three O^{2-} belonging to the fcc structure. Each of the surrounding O^{2-} belongs to the fcc structure if it is surrounded itself by at least three cations of the spinel structure. That means that, on average, the crystallographic coherence between the clustered Ti cations and the surrounding fcc phase is ensured when there are at least nine bonds between its first oxygen neighbors and the cations of the fcc phase. One may then evaluate the number of such bonds for the four-membered clusters.

Each Ti^{4+} of the four-membered clusters is surrounded by three O^{2-}, which are shared with two other titanium cations of the clusters and three O^{2-} shared with sites of the fcc phase only (Figure 8). The three O^{2-} of the first type are surrounded by three Ti^{4+} of the cluster and one A site of the spinel phase; the three other O^{2-} are surrounded by one Ti^{4+} of the cluster and one A site and two B sites of the fcc phase. Each Ti^{4+} of the four-membered cluster has then 12 possible bonds between its surrounding oxygens and the sites in the fcc phase. The probability, p, that each O^{2-}/site pair corresponds to an effective bond can be evaluated from electroneutrality considerations. In the case of a cluster containing four TiO_2 groups, one finds $p = 0.655$. This value has been obtained by writing that the charge −32 of the 16 oxygen anions of the cluster balances the charge +16 of the 4 Ti^{4+} of the cluster; the charge +3/4 16p of the 16p cations on A site and the charge +3.11/6 24p of the 24p cations on the B adjacent sites. For sake of simplicity, it has been assumed that the charge of the fcc cations involved in the bonds corresponds to the average charge found on the A (+3) and B sites (+3.11) and that p was the same for the A and B sites. Then when the cluster contains four TiO_2 groups, there are only $n_{bonds} \approx 7.9$ bonds between the surrounding oxygen of each clustered Ti^{4+} and the cations in the fcc phase. Similarly one finds that when the cluster contains respectively 3, 2, or 1 Ti: $n_{bonds} \approx 9.7$, 11.6, and 13.7. That means that the crystallographic coherence of the cluster with the fcc phase is effectively broken when and only when it contains exactly four Ti atoms. This is precisely what is obtained with the above results: they are the 60% (diffraction data) of the Ti cations belonging to the nondiffracting part of the sample, which gather in clusters containing exactly four TiO_2 entities (EXAFS data).

There are then the structural constraints imposed by the spinel phase, quite unusual at the macroscopic scale when the Fe and Ti are oxidized to their highest valence, which determine the size of the so-formed clusters. In the present case, the impossibility for the Ti cations to reside on the A sites limits the gathering of the Ti cations to a compact structure containing only four TiO_2 entities. This value of four, which is characteristic of the spinel phase, differs from the magic numbers related to special configurations with high thermodynamic stability expected in free clusters: 13, 55, 147, etc. in clusters constituted of rare-gas atoms;[48] 2, 8, 20, 40, etc. in simple metal clusters.[49] Here, the clusters are embedded in a matrix, and the constraint that the Ti cations have to reside on the sites of the spinel structure leads to clusters "living" as four-entity blocks with a break of coherence with the surrounding fcc phase. The present example of embedded TiO_2 clusters is then very similar to vacancy aggregating observed in heavily neutron-irradiated graphite.[50] In this sample indeed, the magic six-membered ring evidenced corresponds to the closed structural unit characteristic of the matrix.

Conclusion

The bulk (Fe, Ti, O) phase diagram is strongly modified at the nanometer scale because of the prohibitive interface energy between the two phases normally present at the micrometer range. For grain size lower than 25 nm, the fcc phase is stabilized instead of the mixture of rhombohedral and pseudo-

brookite phases. The existence of a single phase permits small clusters of TiO_2 to be formed, which cannot happen in micrometer scaled compounds because of cluster growth until phase separation. From a combination of diffraction and absorption spectroscopy experiments, these clusters were carefully characterized: they consist of a compact stack of four TiO_2 entities corresponding to a very stable configuration. Because of the large amount of vacancies lying around the titanium cations, the crystallographic coherence between the fcc phase and the clusters is broken, explaining why the clusters do not participate in the long-range order revealed by diffraction techniques.

References and Notes

(1) Andres, R. P.; Averback, R. S.; Brown, W. L.; Brus, L. E.; Goddard, W. A.; Kaldor, A.; Louie, S. G.; Moscovits, M.; Peercy, P. S.; Riley, S. J.; Siegel, R. W.; Spaepen, F.; Wang, Y. *J. Mater. Res.* **1989**, *4*, 704. Siegel, R. W.; Hu, E.; Cox, D. M.; Goronkin, H.; Jelinski, L.; Koch, C. C.; Roco, M. C.; Shaw, D. T. WTEC Panel Report on Nanostructure Science and Technology; International Technology Research Institute: Baltimore City, MD, 1998.

(2) For reviews, see Gleiter, H. *Nanostruct. Mater.* **1995**, *6*, 3. Siegel, R. W. *Nanostruct. Mater.* **1994**, *4*, 121.

(3) Flashen, S. S. *J. Am. Chem. Soc.* **1955**, *77*, 6194. Uchino, K.; Sadanaga, E.; Hirose, T. *J. Am. Ceram. Soc.* **1989**, *72*, 1555.

(4) Ayyub, P.; Multani, M.; Barma, M.; Palkar, V. R.; Vijayaraghavan, R. *J. Phys. C: Solid State Phys.* **1988**, *21*, 2229.

(5) Garvie, R. C. *J. Phys. Chem. Soc.* **1978**, *77*, 218. Garvie, R. C.; Goss, M. F. *J. Mater. Sci.* **1986**, *21*, 1253.

(6) Skandan, G.; et al. *Nanostruct. Mater.* **1992**, *1*, 313.

(7) McHale, J. M.; Auroux, A.; Perrotta, A. J.; Navrotsky, A. *Science* **1997**, *277*, 788−791.

(8) Blonski, S.; Garofalini, S. H. *Surf. Sci.* **1993**, *295*, 263.

(9) McHale, J. M.; Navrotsky, A.; Perrotta, A. J. *J. Phys. Chem. B* **1997**, *101*, 603.

(10) O'Reilly, W. *J. Magn. Magn. Mater.* **1994**, *137*, 167.

(11) Dieckmann, R.; Schmalzried, H. *Ber. Bunsen-Ges. Phys. Chem.* **1977**, *81*, 344.

(12) Guigue-Millot, N.; Keller, N.; Perriat, P. *Phys. Rev. B* **2001**, *64*(1), article no. 012402.

(13) Taylor, R. W. *J. Am. Cer. Soc.* **1963**, *46*, 278.

(14) Verwey, E. J.; Heilman, E. L. *J. Chem. Phys.* **1947**, *15*, 174.

(15) Readman, P. W.; O'Reilly, W. *J. Geomag. Geoelectr.* **1972**, *24*, 69.

(16) Ozima, M.; Ozima, M. *Phys. Earth Planet. Inter.* **1972**, *5*, 87.

(17) Bernard, F.; Lorimier, J.; Nivoix, V.; Millot, N.; Perriat, P.; Gillot, B.; Berar, J. F.; Niepce, J. C. *J. Solid State Chem.* **1998**, *141*, 105−113.

(18) Néel, L. *Adv. Phys.* **1955**, *4*, 191.

(19) Chevalier, R.; Bolfa, J.; Mathiew, S. *Bull. Soc. Fr. Mineral. Cristallogr.* **1955**, *78*, 307.

(20) Guigue-Millot, N.; Champion, Y.; Hÿtch, M. J.; Bernard, F.; Bégin-Colin, S.; Perriat, P. *J. Phys. Chem. B* **2001**, *105*−*29*, 7125−7132.

(21) Perriat, P.; Gillot, B. *Solid State Ionics* **1993**, *67*, 35−43.

(22) Kester, E.; Gillot, B.; Perriat, P.; Dufour, P. *J. Solid State Chem.* **1996**, *126*, 7−14.

(23) Perriat, P.; Domenichini, B.; Gillot, B. *J. Phys. Chem. Solids* **1996**, *57*−*11*, 1641−1652.

(24) da Fonseca, C.; Traverse, A.; Tadjeddine, A.; da Cunha Belo, M. *J. Electroanal. Chem.* **1995**, *388*, 115−122.

(25) Lengeler, B.; Eisenberger, P. *Phys. Rev. B* **1980**, *21*, 4507.

(26) Michalowicz, A. Logiciels pour la chimie, no. 102, Société Française de Chimie, Paris, 1991.

(27) Koningsberger, D. C.; Prins, R. *X-ray Absorption*; J. Wiley: New York, 1986.

(28) McKale, A. G.; Knapp, G. S.; Chan, S. K. *Phys. Rev. B* **1986**, *33*, 841.

(29) Bernard, F.; Lorimier, J.; Nivoix, V.; Millot, N.; Niepce, J. C.; Perriat, P.; Gillot, B.; Ferlet, M.; Berar, J. F. *Mater. Sci. Forum* **1998**, *278*−*281*, 594.

(30) http://www-llb.cea.fr/fullweb/poudres.htm

(31) Langford, J. I.; Special publication 846; National Institute of Standards and Technology: Gaithersburg, MD, 1992; p 145.

(32) Halder, N. C.; Wagner, C. N. J. *Adv. X-ray Anal.* **1966**, *9*, 91.

(33) Gillot, B.; Jemmali, F. *Mater. Chem. Phys.* **1986**, *15*, 577−588.

(34) Ishii, M.; Nakahira, M.; Yamanaka, T. *Solid State Commun.* **1972**, *11*, 209.

(35) Donnay, J. D. H.; Turrell, G. *Chem. Phys.* **1974**, *6*, 1.

(36) Perriat, P.; Niepce, J. C.; Caboche, G. *J. Therm. Anal.* **1994**, *41*, 635−649.

(37) Perriat, P. *Nanostruct. Mater.* **1995**, *6*, 791−794.

(38) Handbook of Chemistry and Physics, 61st edition (1980−1981), CRC Press: Boca Raton, FL; D-71.

(39) Poix, P.; Basile, F.; Djega-Mariadassou, C. *Ann. Chim.* **1975**, *3*, 175−184.

(40) Poix, P.; Liaisons atomioques et propriétés physiques des composés minéraux, ed. Suchet, Paris 1966 186.

(41) Rietveld, H. M. *J. Appl. Crystallogr.* **1969**, *2*, 65.

(42) *International Tables for Crystallography: Vol. A Space-group symmetry*; Hahn, T., Ed.; Kluwer Academic Publishers: Dordrecht/Boston/London, 1989; pp 686−693.

(43) Warren, B. E. *X-ray diffraction*; Addison-Wesley: Reading, MA, 1990.

(44) Watson, R. E.; Freeman, A. J. *Acta Crystallogr.* **1961**, *14*, 27.

(45) Teillet, J.; Bouree, F.; Krishnan, R. *J. Magn. Magn. Mater.* **1993**, *123*, 93−96.

(46) Uozumi, T.; Okada, K.; Kotani, A.; Durmeyer, O.; Kappler, J. P.; Beaurepaire, E.; Parlebas, J. C. *Europhys. Lett.* **1992**, *18*, 85.

(47) Bair, R. A.; Goddard, W. A. *Phys. Rev. B* **1980**, *22*, 2767.

(48) Miehle, W.; et al. *J. Chem. Phys.* **1989**, *91*, 5940.

(49) Knight, W. D.; et al. *Phys. Rev. Lett.* **1984**, *52*, 2141.

(50) Tang, Z.; et al. *Phys. Rev. Lett.* **1999**, *82*, 2532−2535.

(51) Perriat, P.; Fries, E.; Millot, N.; Domenichini, B. *Solid State Ionics* **1999**, *117*, 175−184.